JACS
JOURNAL OF THE AMERICAN CHEMICAL SOCIETY
Article
pubs.acs.org/JACS

Pyridine *N*-Oxide vs Pyridine Substrates for Rh(III)-Catalyzed Oxidative C−H Bond Functionalization

Sharon R. Neufeldt,[†] Gonzalo Jiménez-Osés,[†] John R. Huckins,*[,‡] Oliver R. Thiel,*[,‡] and K. N. Houk*[,†]

[†]Department of Chemistry and Biochemistry, University of California, Los Angeles, California 90095, United States
[‡]Process Development, Amgen Inc., One Amgen Center Drive, Thousand Oaks, California 91320, United States

Supporting Information

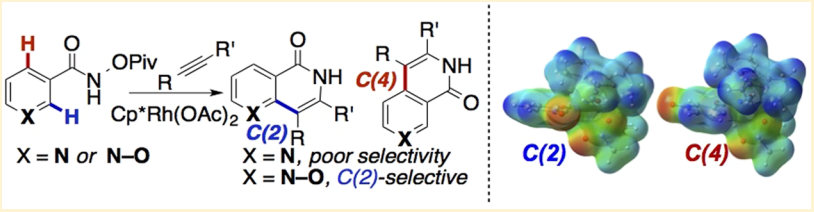

ABSTRACT: The origin of the high reactivity and site selectivity of pyridine *N*-oxide substrates in *O*-pivaloyl hydroxamic acid-directed Rh(III)-catalyzed (4+2) annulation reactions with alkynes was investigated computationally. The reactions of the analogous pyridine derivatives were previously reported to be slower and to display poor site selectivity for functionalization of the C(2)−H vs the C(4)−H bonds of the pyridine ring. The *N*-oxide substrates are found to be more reactive overall because the directing group interacts more strongly with Rh. For *N*-oxide substrates, alkyne insertion is rate-limiting and selectivity-determining in the reaction with a dialkyl alkyne, but C−H activation can be selectivity-determining with other coupling partners such as terminal alkynes. The rates of reaction with a dialkyl alkyne at the two sites of a pyridine substrate are limited by two different steps: C−H activation is limiting for C(2)-functionalization, while alkyne insertion is limiting for C(4)-functionalization. Consistent with the observed poor site selectivity in the reaction of a pyridine substrate, the overall energy barriers for functionalization of the two positions are nearly identical. High C(2)-selectivity in the C−H activation step of the reaction of the *N*-oxide is due to a cooperative effect of the C−H Brønsted acidity, the strength of the forming C−Rh bond, and intramolecular electrostatic interactions between the [Rh]Cp* and the heteroaryl moieties. On the other hand, some of these forces are in opposition in the case of the pyridine substrate, and C(4)−H activation is moderately favored overall. The alkyne insertion step is favored at C(2) over C(4) for both substrates, and this preference is largely influenced by electrostatic interactions between the alkyne and the heteroarene. Experimental results that support these calculations, including kinetic isotope effect studies, H/D exchange studies, and results using a substituted pyridine, are also described.

INTRODUCTION

Rh(III)-catalyzed C−H activation is an attractive strategy for constructing new C−C bonds due to the high functional group tolerance of Rh(III) and the remarkable diversity of products that can be accessed in this way.[1] For aromatic substrates containing protic directing groups (−NH or −OH), 1:1 coupling with alkenes and alkynes typically occurs to provide substituted 5- or 6-membered heterocycles via formation of a C−C and an N−C or O−C bond.[2] This class of transformations was first developed using carboxylic acid[3] or amide[4] directing groups on benzene in the presence of an external oxidant [e.g., Cu(II) and air, Scheme 1A]. More recent examples employ substrates containing N−O[5] (e.g., hydroxamic acids, oximes) or N−N[6] bonds (e.g., hydrazines) that serve a dual role both as a directing group and as an oxidant for Rh (e.g., Scheme 1C).[7]

Analogous annulation reactions have been performed using directing-group-containing electron-rich heterocycles (e.g., pyrroles, furans, and thiophenes),[4b,c,5a−f,m−o] as well as 2- or 4-substituted pyridines containing only one possible site for directed C−H activation.[8] However, examples of Rh(III)-catalyzed C−H functionalization of 3-substituted pyridines are rare and suffer from poor reactivity and/or poor site selectivity (Scheme 2).[4b,f,5d,9]

Recently, we reported a Rh(III)-catalyzed annulation of heterocycle substrates containing two possible sites of C−H activation.[10] *O*-Pivaloylhydroxamic acid derivatives of nicotinamides (**1a**, Scheme 3) undergo conversion to naphthyridinone products using norbornene or 4-octyne as coupling partners. This reaction exhibits only modest site selectivity, with a small preference for C−C coupling at the 2-position of the pyridine ring (e.g., 1.7:1 using 4-octyne). The poor selectivity is consistent with the ∼1:1 selectivity observed by Glorius in the analogous reaction using an allene instead of an alkyne (Scheme 2B).[5d] Moreover, compared to literature reports of the analogous reaction of carbocyclic substrates (benzhydroxamic acid derivatives),[5b] functionalization of the pyridine

Received: April 4, 2015
Published: July 21, 2015

DOI: 10.1021/jacs.5b03535
J. Am. Chem. Soc. 2015, 137, 9843−9854

Scheme 1. Rh(III)-Catalyzed Annulations of Substituted Benzenes by Directed C−H Activation[3,4b,5b]

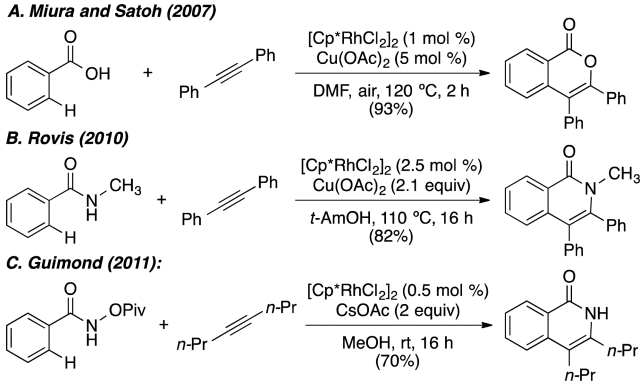

Scheme 2. Rh(III)-Catalyzed C−H Functionalization of Nicotinamide Derivatives[4b,5d,9]

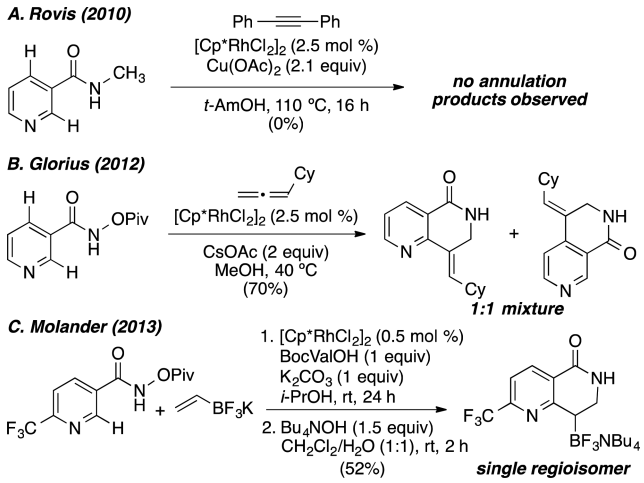

Scheme 3. Rh(III)-Catalyzed Annulations of Nicotinamide Derivatives[10]

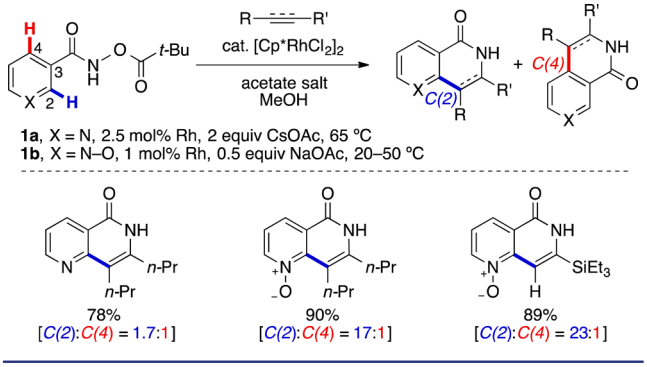

ring requires higher temperatures and catalyst loadings to achieve an acceptable reaction rate. In contrast, the *N*-oxide[11−15] derivatives (**1b**) undergo the desired annulation reactions with high site selectivity (typically >20:1) for the 2-position of the *N*-oxide ring. These reactions often proceed at room temperature and with lower catalyst loadings.

The mechanism of Rh(III)-catalyzed (4+2) annulation of benzhydroxamic acid derivatives with acetylene has been studied experimentally and computationally by Guimond, Gorelsky, and Fagnou (Scheme 4A),[5b] and the analogous reaction with ethylene has been studied computationally by Xia et al.[16,17] The C−H activation step was calculated to be turnover-limiting and to proceed through a concerted metalation−deprotonation (CMD) mechanism involving a neutral Rh(III) species.[18,19] Only one C−H bond is available for activation in these systems; as such, the site selectivity of Rh(III)-catalyzed anionic ligand-directed C−H functionalization has not been explored computationally. Furthermore, little is known about the relative reactivity of different C−H bonds within heterocyclic substrates toward Rh(III)-catalyzed C−H functionalization involving protic directing groups.[20]

Scheme 4. Rh(III)-Catalyzed (4+2) Annulation Studied Computationally (A) by Guimond, Gorelsky, and Fagnou and (B) in This Work[5b]

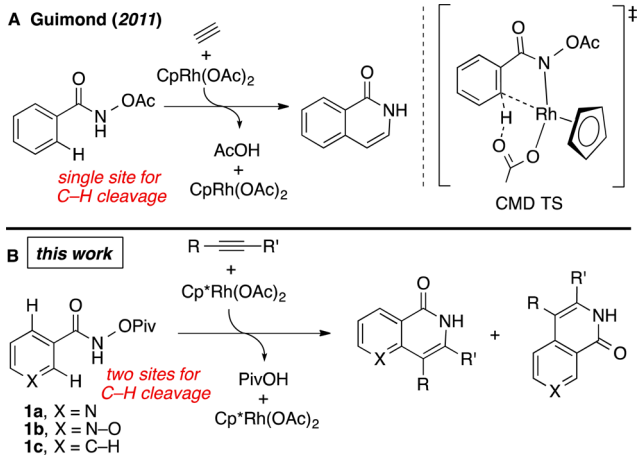

We have now used density functional theory (DFT) calculations to investigate the origin of the reactivity and site-selectivity differences between pyridine and pyridine *N*-oxide substrates **1a** and **1b** toward Rh(III)-catalyzed (4+2) annulations with alkynes (Scheme 4B). For reference, we also performed calculations with the analogous benzamide substrate **1c** (see Supporting Information), which resembles the system previously studied by Guimond.[5b] We describe the influence of both substrate and alkyne partner on the identity of the rate- and selectivity-determining steps, and provide an explanation of the factors controlling the site selectivity of the directed C−H activation and the alkyne insertion steps. Corroborating kinetic isotope effect and H/D exchange studies, as well as results with a substituted pyridine substrate, are also reported.

COMPUTATIONAL METHODS

Calculations were performed with Gaussian 09.[21] For all calculations except the acidity calculations shown in Scheme 6, geometry optimizations of minima and transition states were carried out in the gas phase with the M06 functional[22] and the LANL2DZ pseudopotential[23] for Rh and the 6-31G(d) basis set for all other atoms. An ultrafine integration grid was used and was found to be important for reproducing experimental results. Frequency analyses were carried out at the same level to evaluate the zero-point vibrational energy and thermal corrections at 298 K (or 338 K for **1a** and its complexes). The nature of the stationary points was determined in each case according to the appropriate number of negative eigenvalues of the Hessian matrix. Where necessary, mass-weighted intrinsic reaction coordinate (IRC) calculations were carried out by using the Gonzalez and Schlegel scheme in order to ensure that the TSs indeed connect the appropriate reactants and products.[24] Single-point energies were obtained using the M06 functional with the SDD[25] pseudopotential for Rh, augmented with two f-type polarization functions,[26] and with the 6-311+G(2d,p) basis set for all other atoms.

DOI: 10.1021/jacs.5b03535
J. Am. Chem. Soc. 2015, 137, 9843−9854

Scheme 5. Proposed Catalytic Cycle for the Rh(III)-Catalyzed (4+2) Annulation Reaction of 1 with an Alkyne

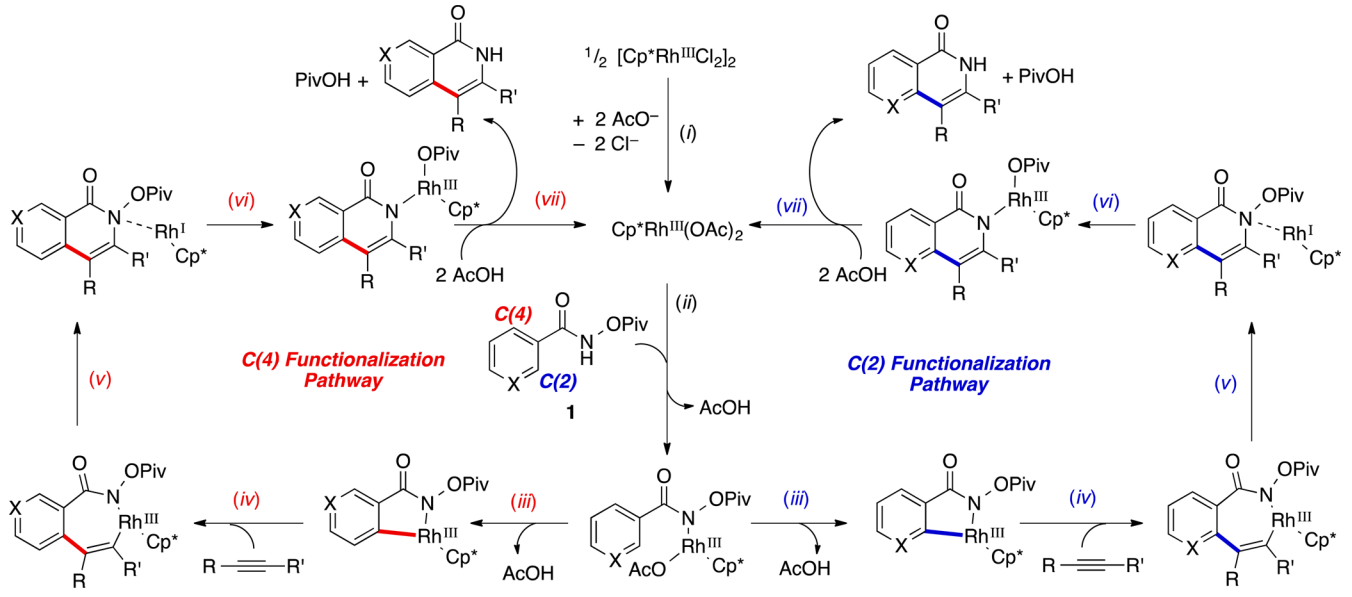

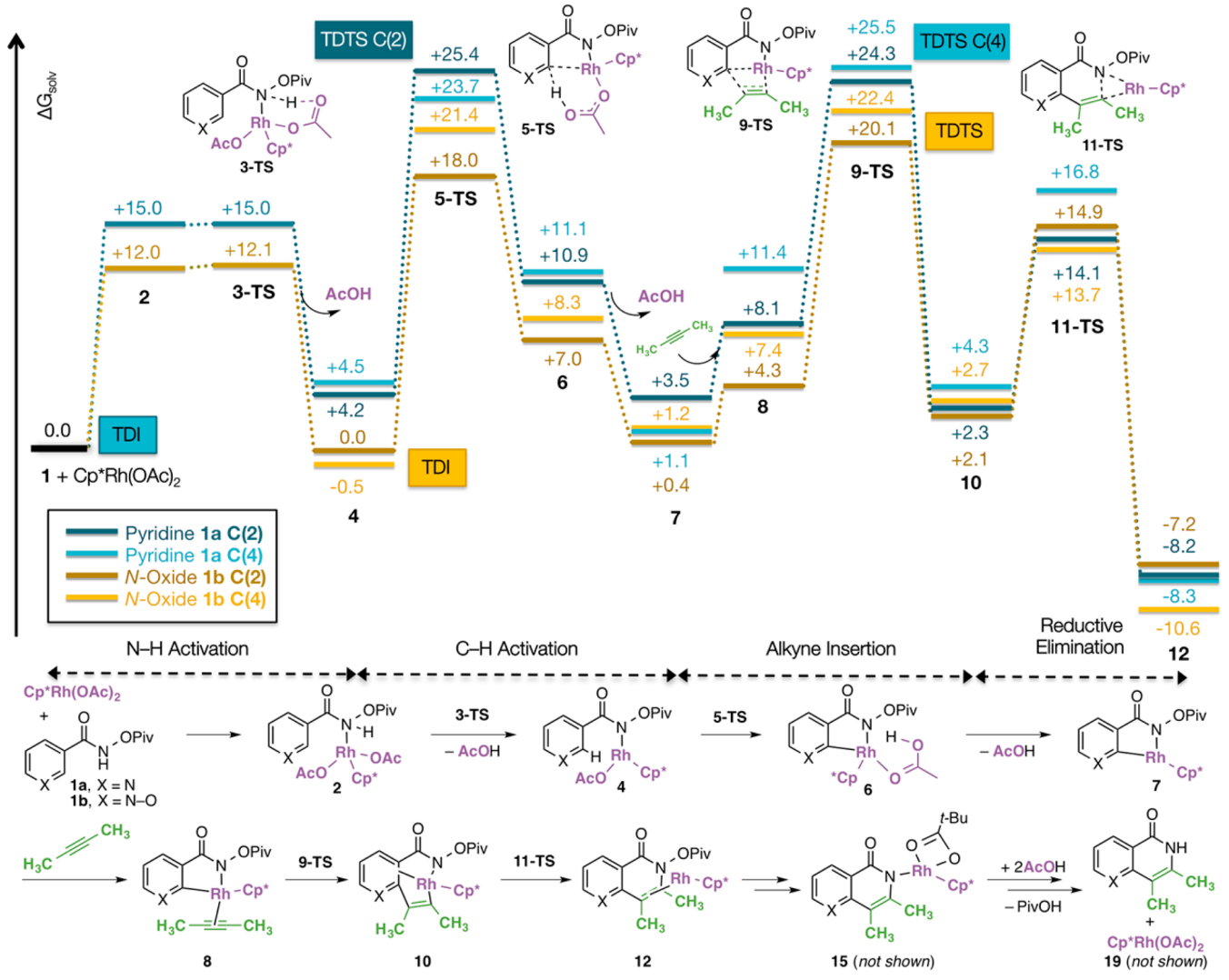

Figure 1. Free energy profiles for the first half of the catalytic cycle for the Rh(III)-catalyzed (4+2) annulation reaction of **1a** and **1b** with 2-butyne. Free energies are given in kcal mol^{-1}.

DOI: 10.1021/jacs.5b03535
J. Am. Chem. Soc. 2015, 137, 9843−9854

Bulk solvent effects in MeOH were considered implicitly by performing single-point energy calculations on the gas-phase optimized geometries through the SMD polarizable continuum model.[27] For the acidity calculations shown in Scheme 6, geometry optimizations and frequency calculations were carried out in the solvent phase (MeOH) with the M06-2X[22a] functional and the 6-311+G(2d,p) basis set using IEF-PCM.[28] The 3D structures in Figures 2, 4, and 7 were prepared using CYLView.[29]

RESULTS AND DISCUSSION

The proposed catalytic cycle for the (4+2) coupling between substrates **1** and an alkyne is depicted in Scheme 5. The cycle comprises the following steps: (i) breakup of the Rh chloride dimer by acetate anion to give the active catalyst Cp*Rh(OAc)$_2$ (Cp* = pentamethylcyclopentadienyl),[20,30] (ii) N−H activation (deprotonation) and loss of AcOH to provide a Rh−amidate intermediate, (iii) C−H activation at either C(2) or C(4) and loss of AcOH, (iv) alkyne insertion into the Rh−C bond, (v) C−N bond-forming reductive elimination, (vi) re-oxidization of Rh(I) to Rh(III), and (vii) amide protonation and ligand exchange to give the final naphthyridinone product and regenerate the active catalyst.

Calculated Reactivity and Site Selectivity of Pyridine 1a vs *N*-Oxide 1b in the Reaction with 2-Butyne. The full catalytic cycles of the reactions of pyridine **1a**, *N*-oxide **1b**, and benzamide **1c** with 2-butyne were calculated. This alkyne was chosen as a model for 4-octyne, an alkyne that has been successfully coupled with all three substrates experimentally.[5b,10] The individual steps of the calculated mechanisms resemble those previously presented by Guimond et al. for the reaction of a non-heterocyclic model substrate with acetylene (Scheme 1A).[5b]

The gold lines in Figure 1 depict the first portion of the free energy profile for the reaction of *N*-oxide **1b** with 2-butyne (see the Supporting Information for the full catalytic cycle). When all steps are considered, including the remaining later steps that are not shown, alkyne insertion is the turnover-determining transition state (TDTS) for functionalization at either position. The turnover-determining intermediate (TDI) for both reaction pathways is Rh(III)−amidate complex **4b-iv**. These species represent the two states that are separated by the maximum energetic span in the forward direction along the catalytic cycle,[31] equal to 20.6 and 22.9 kcal mol^{-1} for C(2)- (dark gold) and C(4)-functionalization (light gold), respectively.[32] By comparing the differences in the energetic spans of the two free energy surfaces ($\Delta\Delta G^{\ddagger}$ = 2.3 kcal mol^{-1}), the selectivity using 2-butyne as a model for 4-octyne is in good agreement with experiment. The calculated product ratio is ~49:1 in favor of C(2)-functionalization, and the experimentally observed product ratio in the reaction of **1b** with 4-octyne is 17:1 (experimental $\Delta\Delta G^{\ddagger} \approx$ 1.7 kcal mol^{-1}).[33]

The turnover-limiting alkyne insertion step stands in contrast to Guimond's calculated rate-limiting C−H activation step in the reaction of a model benzamide substrate shown in Scheme 4A.[5b] Interestingly, we calculate that alkyne insertion is also turnover-limiting for benzamide **1c** (see Supporting Information). Our computed energetics differ from the previous work due to substrate differences and our use of a larger model system (a disubstituted alkyne instead of acetylene, and Cp* as a ligand). Our calculations also consider dispersion forces (see Computational Methods section), which have been shown to be important for obtaining good agreement between experiment and computation in related organometallic systems.[18,20,22,34]

Pyridine **1a** is experimentally less reactive than *N*-oxide **1b**. The free energy surface for the reaction of **1a** with 2-butyne (Figure 1, dark and light blue lines for 2- and 4-functionalization, respectively) resembles that of **1b**. Alkyne insertion (**9a-TS**) is turnover-limiting for C(4)-functionalization, but C−H activation (**5a-TS**) is the slow step for C(2)-functionalization. The energy span for C(2)-functionalization of **1a** is 25.4 kcal mol^{-1}, and the energy span for C(4)-functionalization is 25.5 kcal mol^{-1}. The negligible energy difference between these two pathways gives an estimated product ratio of nearly 1:1, only slightly favoring 2-functionalization. This ratio is consistent with the experimentally observed poor site selectivity for the reaction of **1a** with 4-octyne (product ratio = 1.7:1 favoring 2-functionalization, Scheme 3).[35]

The enhanced reactivity of the *N*-oxide relative to pyridine is apparent when comparing the free energy surfaces for the two substrates. In the first part of the catalytic cycle (prior to the formation of intermediate **10**), the intermediates and transition states along the reaction pathway of *N*-oxide **1b** are generally about 3−5 kcal mol^{-1} lower in energy than the corresponding states of pyridine **1a**, as measured from the separated reactants (substrate and catalyst). Stated another way, the Rh−amide interaction, featured in the complexes in the early part of the catalytic cycle, is apparently stronger for the *N*-oxide complexes. The explanation for these stronger Rh−N interactions is likely the more electron-withdrawing character of the pyridine *N*-oxide ring.[36] This property leads to greater delocalization of the amide nitrogen electron density, resulting in a softer, more polarizable ligand with enhanced affinity toward Rh.

This Rh−N interaction is illustrated in the minimum energy complexes **4** (Figure 2). The Roman numerals **ii** and **iv** indicate structures that lie along the pathway for functionalization at the

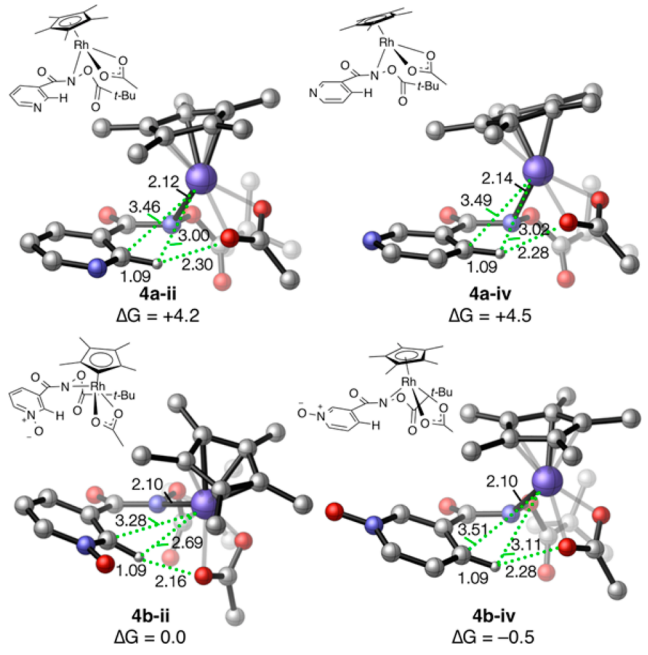

Figure 2. Lowest energy structures of the Rh−amidate intermediates **4**. Free energies relative to the separated reactants are given in kcal mol^{-1} and distances in angstroms.

DOI: 10.1021/jacs.5b03535
J. Am. Chem. Soc. 2015, 137, 9843−9854

2- and the 4-positions of the heterocycle, respectively. The anionic amidate ligand coordinates more tightly to Rh in the *N*-oxide complex **4b**, as reflected by the slightly shorter Rh–N distances (e.g., 2.10 Å in **4b** vs 2.12–2.14 Å in **4a**, Figure 2).

Change in TDTS of the Reaction of *N*-Oxide 1b with Different Alkynes. Our calculations predict that the turnover- and selectivity-determining step of the reaction of the *N*-oxide can be either C–H activation or alkyne insertion, depending on the identity of the alkyne (Figure 3). The left side of Figure 3

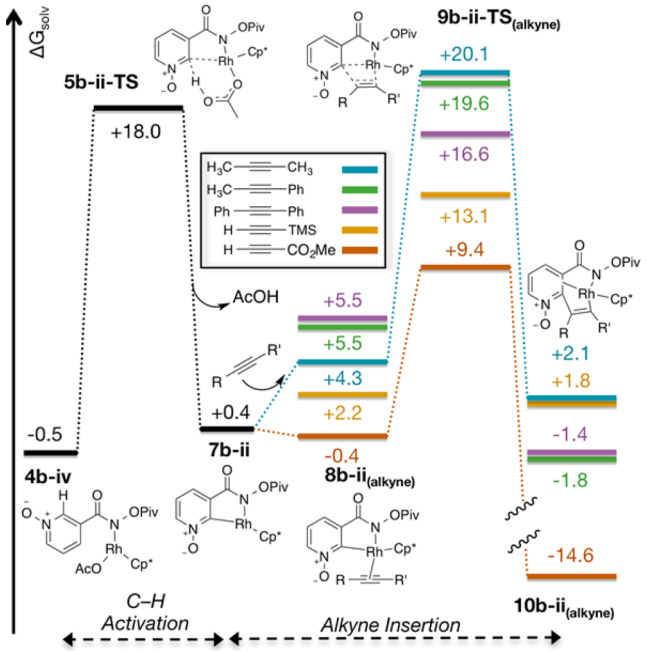

Figure 3. Change in turnover-determining transition state (C–H activation vs alkyne insertion) for the annulation reaction of **1b** with various alkynes. Free energies relative to the separated reactants are given in kcal mol^{-1}. Intermediate **6b** has been omitted for clarity.

(black lines) depicts the free energy profile for C–H activation at the experimentally preferred 2-position of *N*-oxide **1b**. The right side of Figure 3 shows the free energy for insertion of various alkynes into rhodacycle **7b-ii**. When the alkyne is 2-butyne (blue) or 1-phenyl-1-propyne (green), alkyne insertion is a higher energy process than C–H activation. Under these circumstances, our calculations indicate that C–H activation is, in principle, reversible. This result is in agreement with the partial incorporation (8%) of deuterium at C(2) of **1b** observed experimentally in the reaction with a dialkyl alkyne run to partial conversion (eq 1).[37] In such cases, selectivity depends primarily on the relative energies of the alkyne insertion transition states for 2- vs 4-functionalization.

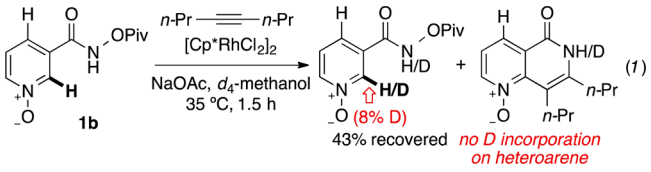

On the other hand, alkyne insertion is a slightly lower energy process with diphenylacetylene (Figure 3, purple), and is particularly facile with terminal alkynes TMS-acetylene (gold) and methylpropiolate (orange). In these cases, C–H activation is calculated to be irreversible, and selectivity is determined at the C–H activation step. This prediction is supported experimentally by the failure to observe any H/D exchange in the remaining starting material in the reaction of **1b** with TES-acetylene in d_4-methanol run to partial conversion (eq 2).

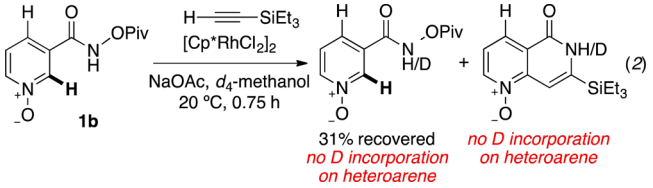

The experimentally observed change in site selectivity (albeit modest) using different alkynes is also consistent with the change in the computed selectivity-determining step. The reaction with TMS-acetylene gives slightly higher selectivity (>20:1) than the reaction with 4-octyne (17:1),[10] in keeping with the C–H activation step ($\Delta\Delta G^{\ddagger}_{(C4-C2)}$ = 3.4 kcal mol^{-1}) being more selective than insertion of an internal alkyne ($\Delta\Delta G^{\ddagger}_{(C4-C2)}$ = 2.3 kcal mol^{-1} for 2-butyne).

On the basis of the computed energy profiles and the irreversibility of C–H activation in the presence of TMS-acetylene, we predicted that a kinetic isotope effect (KIE) should be observed experimentally in the reaction of a silyl acetylene, reflecting the relative rates of C–H vs C–D bond cleavage. The calculated k_H/k_D for the C(2)–H activation step of *N*-oxide **4b** is 5.5 at room temperature. Indeed, when equimolar amounts of **1b** and d_4-**1b** were submitted to the reaction conditions using TES-acetylene, a competition KIE of 4.4 [measured by ^{1}H nuclear magentic resonance (NMR) spectroscopy] or 3.8 [measured by high-resolution mass spectrometry (HRMS)] was observed (eq 3).

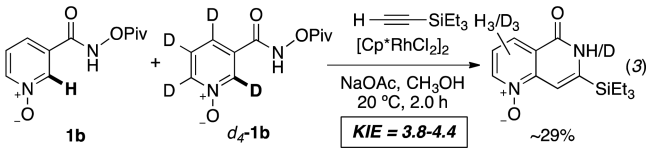

On the other hand, alkyne insertion, not C–H activation, is calculated to be turnover-limiting with our model dialkyl alkyne. Nevertheless, we expected that a KIE would still be observed in the reaction of **1b** with 4-octyne, albeit of a smaller magnitude, due to the similarity in the energy barriers for C–H activation and alkyne insertion. The KIE observed for the reaction using 4-octyne was smaller than seen with TES-acetylene [KIE = 3.4 in CH_3OH (HRMS and NMR), or 2.5 (HRMS) or 2.9 (NMR) in CD_3OD, eq 4], which is consistent with a higher-energy alkyne insertion step allowing for partial equilibration of the intermediates before and after C–H activation.[38]

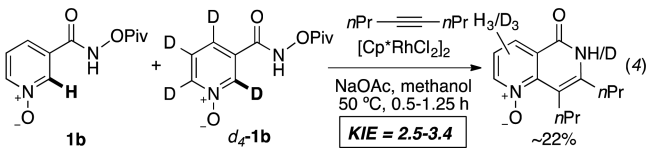

Origin of Selectivity of C–H Bond Activation. C–H activation takes place through a six-centered intramolecular CMD mechanism (Figure 4). The especially high reactivity of the C(2)–H bond of the *N*-oxide ($\Delta G^{\ddagger}$ = 18.5 kcal mol^{-1}) makes C–H activation at this site particularly favorable,

DOI: 10.1021/jacs.5b03535
J. Am. Chem. Soc. 2015, 137, 9843–9854

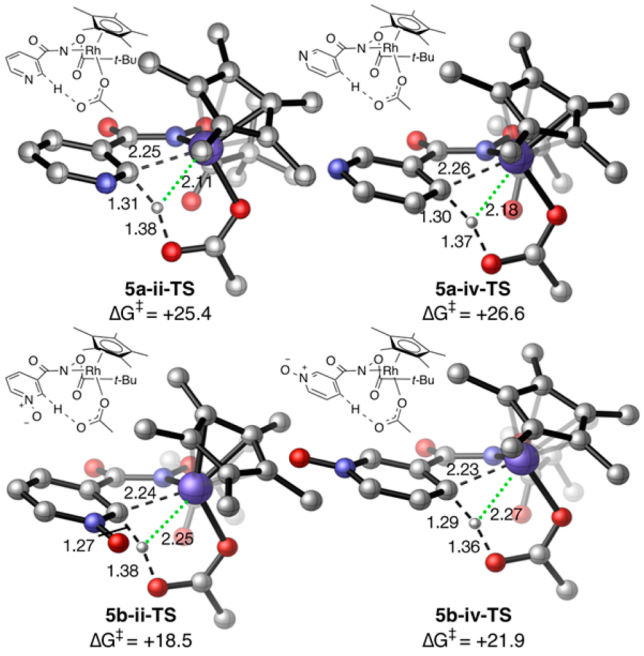

Figure 4. Geometries of the minimum energy CMD transition structures **5-TS**. Free energies relative to the turnover-determining intermediate (separated reactants for **5a**, **4b-iv** for **5b**) are given in kcal mol^{-1} and distances in angstroms.

increasing both reactivity and site selectivity. However, the geometries of the lowest-energy C−H activation transition structures for the 2- and 4-positions of the pyridine and pyridine *N*-oxide are nearly identical, which complicates rationalization of the computed selectivity.

IRC calculations show that the C−H activation mechanism is energetically concerted but highly asynchronous. C−Rh bond formation is continuous as the fragments approach (gold line, Figure 5), but the C−H bond breaks abruptly, starting just before the highest energy point on the reaction coordinate (orange line). This observation suggests that the attraction between catalyst and substrate are of equal, if not greater, importance than the inherent weakness of different C−H bonds toward heterolytic cleavage.

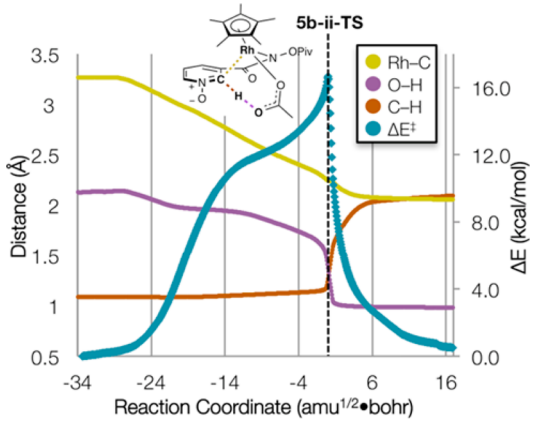

Figure 5. Electronic energy (ΔE) and calculated bond distances along the intrinsic reaction coordinate of C−H activation of *N*-oxide **1b** at the 2-position (transition state **5b-ii-TS** is at position 0 on the reaction coordinate).

Previous DFT studies on Pd-catalyzed C−H activation of heteroarene *N*-oxides that do not contain a directing group[39] have suggested that the strength of the developing C−M bond,[39c] C−H acidity,[39d] heteroarene distortion,[39a,b,d] and carbon nucleophilicity[39e] may influence the site selectivity of C−H activation. Gorelsky and Fagnou studied the reactivity of a wide range of (hetero)aromatic substrates toward undirected Pd(II)-catalyzed C−H activation by a CMD mechanism.[39a,b,d] They concluded that Brønsted acidity only sometimes parallels reactivity.[39d] Instead, they found that a distortion−interaction model better explained the observed reactivities. Related to this, it is apparent that the geometry of intermediate **4b-ii** in our system bears a much closer resemblance to its corresponding transition structure **5b-ii-TS** than does any other intermediate **4** to its respective **5-TS** (compare Figures 2 and 4). As such, the shorter C−H···OAc and C···Rh distances in **4b-ii** suggest that the distortion required to achieve the TS geometry of **5b-ii-TS** is the lowest of all of the calculated reaction pathways (given that the cleaving C−H and forming C−Rh bond distances are essentially identical in all of the calculated TSs). However, because quantitative distortion−interaction analysis is not easily conducted with intramolecular reactions, we approached the task of understanding the relative energies of the C−H activation transition states by exploring other diverse factors.

We have identified three key factors that may influence the reactivity of different C−H bonds toward intramolecular activation at Rh(III) in these systems: (1) Brønsted acidity of the C−H bond, (2) strength of the forming C−Rh bond, and (3) electrostatic interactions between the Rh catalyst fragment (especially the Cp* ligand) and the pyridine or pyridine *N*-oxide ring. In the case of the *N*-oxide substrate, all three of these factors work cooperatively to favor C(2)−H activation. In contrast, although electrostatics favor C(2)−H activation of the pyridine ring, acidity and C−Rh bond strength favor the opposite selectivity [C(4)−H bond cleavage].

The relative acidities of the different C−H bonds were derived from the computed thermodynamics of model acid−base reactions involving intermolecular deprotonation of the simple heterocycles pyridine and pyridine *N*-oxide at C(2) and C(4) by acetate (Scheme 6A). For both heterocycles, the C−H bond that is energetically favored for activation in **5-TS** corresponds to the more acidic proton. Overall, pyridine *N*-

Scheme 6. Comparison of Pyridine and Pyridine *N*-Oxide C−H Bond Acidities with Free Energy Barriers to C−H Activation

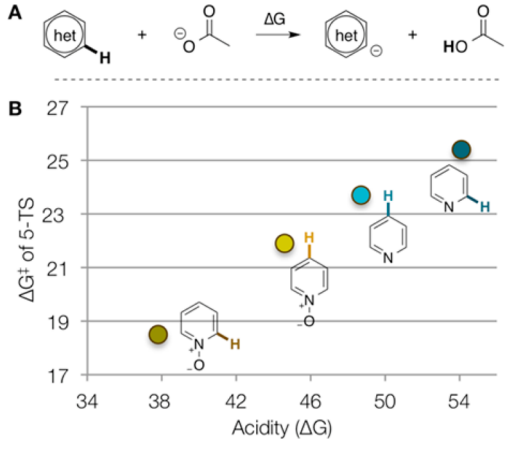

DOI: 10.1021/jacs.5b03535
J. Am. Chem. Soc. 2015, 137, 9843−9854

oxide is more acidic than pyridine, with the *N*-oxide C(2)–H being the most acidic proton in our study (smallest ΔG of deprotonation).[40] In contrast, the C(4)–H of pyridine is more acidic than the C(2)–H.[41] A plot of the free energies of deprotonation vs C–H activation shows good correlation between the two parameters (Scheme 6B). As such, the selectivity of C–H activation trends with Brønsted acidity.

The trends in C–Rh bond strengths were estimated by calculating the change in free energy upon separating model rhodacycles into their substrate and metal fragments by homolytic cleavage of the Rh–C bond (Scheme 7A; see Supporting Information for a discussion on the choice of model complexes). In general, the pyridine *N*-oxide forms stronger bonds to Rh than does pyridine. Whereas the *N*-oxide C(2)–Rh bond is stronger than the corresponding C(4)–Rh bond, the trend is reversed for pyridine: the pyridine C(4)–Rh bond is stronger than C(2)–Rh. As seen with acidity, C–Rh bond strengths also correlate well with the free energy barriers to C–H activation (Scheme 7B).[39c,42]

Scheme 7. Comparison of C–Rh Bond Dissociation Energies (BDE) with Free Energy Barriers to C–H Activation

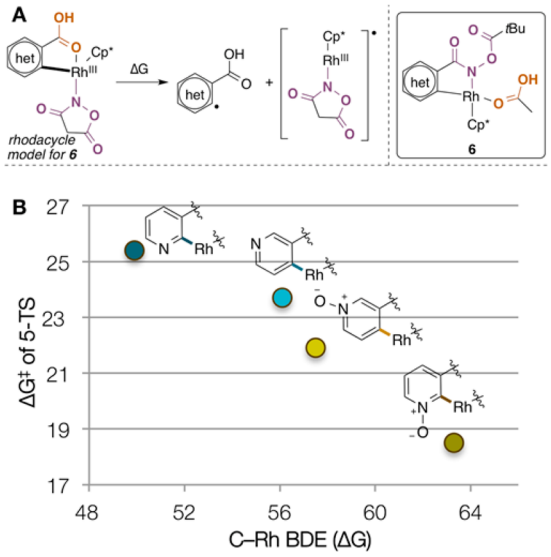

The rationalization for the observed trends in acidity and C–Rh bond strength lies in the electronic properties of the heteroaromatic rings. The presence of the electronegative oxygen atom on the *N*-oxide depletes charge from the nitrogen (NBO[43] charges q_N = −0.47 and +0.08 *e* in pyridine and pyridine *N*-oxide, respectively). This more positive nitrogen of the *N*-oxide leads to a slightly higher polarization of the heteroaryl C–H bonds through inductive effects (Δq_{H2-C2} = +0.14 vs +0.24 *e* in pyridine and pyridine *N*-oxide, respectively). Notably, this polarization can explain the unusually short C–H···OAc distance in pre-transition-state complex **4b-ii**, as described above. The lack of electron density in the nitrogen of the *N*-oxide favors the allocation of negative charge at C(2) developed upon heterolytic deprotonation (i.e., higher acidity as in Scheme 6). On the other hand, development of negative charge at C(2) of pyridine is disfavored due to electron repulsion by the lone pair of the adjacent nitrogen. Homolytic dissociation of the C(2)–Rh bond of the corresponding rhodacycle would generate an unstable radical adjacent to the electron-deficient nitrogen of the *N*-oxide, which explains the large C(2)–Rh bond dissociation energy calculated for the *N*-oxide.

Lastly, electrostatic interactions in the transition state complexes for C–H activation appear to play a role in the relative energetics of the two sites. Although the geometries of the C–H activation transition states (**5-TS**) are essentially identical, their dipole moments in MeOH differ markedly (Table 1). The transition structures for C(2)–H activation of both substrates are significantly less polar than those for C(4)–H activation. Moreover, the transition states for C(2)–H activation involve a *decrease* in polarity compared to the lowest energy conformation of the preceding intermediates, whereas C(4)–H activation requires an *increase* in polarity when moving from intermediate **4** to the transition state ($\Delta\mu$). These data indicate the existence of favorable electrostatic interactions in the transition states for C(2)–H activation in both the pyridine substrate **1a** and its *N*-oxide **1b**, with particular significance in the latter case.

Table 1. Calculated Dipole Moments of Rh–Amidate Intermediates 4 and C–H Activation Transition Structures 5-TS in MeOH

entry	C–H bond broken in TS	**4** μ (D)	**5-TS** μ (D)	Δμ (D)[a]
1	 **a-ii**	14.0	11.9	−2.1
2	 **a-iv**	14.7	17.2	+3.2
3	 **b-ii**	13.5	13.0	−3.4
4	 **b-iv**	16.4	18.8	+2.4

[a] $\Delta\mu$ is the change in dipole moment from minimum energy complex **4** (**4a-ii** for the pyridine substrate, and **4b-iv** for the *N*-oxide substrate) to the indicated transition state **5-TS**. Note that for entry 3, this means that $\Delta\mu$ is calculated as $\mu_{(5b\text{-}ii\text{-}TS)} - \mu_{(4b\text{-}iv\text{-}TS)}$ = 13.0 D − 16.4 D.

To examine these electrostatic interactions in more detail, we optimized a model Rh–amidate complex **4d** in which a hydrogen replaces the heteroaryl ring that would be present in **4a** or **4b** (Figure 6A). Thus, the dipole moment of model complex **4d** is not influenced by any heteroaryl ring. The dipole moment of this structure is relatively large (μ = 15.1 D in MeOH), and the dipole vector (not shown) is oriented with the positive end near the center of the Cp* ring and the negative end near the amide and pivalate carbonyl oxygens. The polarity of **4d** is further illustrated by its electrostatic potential surface (Figure 6A).

The electron density in both isolated heteroarenes is accumulated in the N (pyridine) and O (pyridine *N*-oxide) atoms, and the dipole of pyridine *N*-oxide is significantly larger than that of pyridine (Figure 6B). Thus, in the C(2)–H transition structures **5a-ii-TS** and **5b-ii-TS** (which can be loosely approximated as a composite of **4d** and pyridine or pyridine *N*-oxide), the more electron-rich (red) region of the

DOI: 10.1021/jacs.5b03535
J. Am. Chem. Soc. 2015, 137, 9843–9854

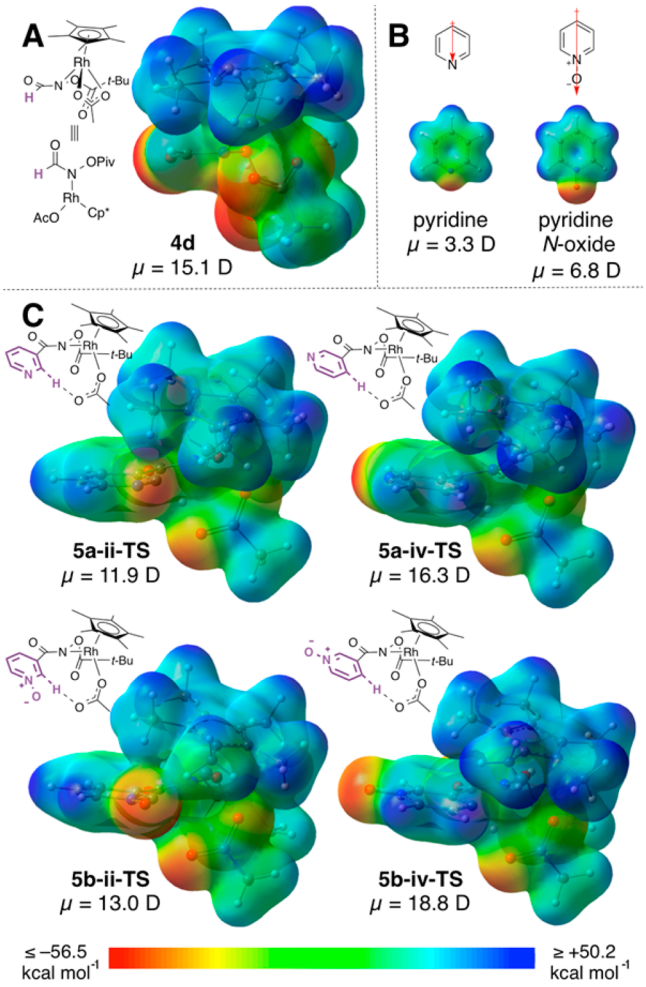

Figure 6. Electrostatic potential surfaces and dipole moments of (A) Rh−amidate model complex **4d** lacking a heteroaryl ring, (B) pyridine and pyridine *N*-oxide, and (C) transition structures for C−H activation **5-TS**. Dipole moments calculated in MeOH.

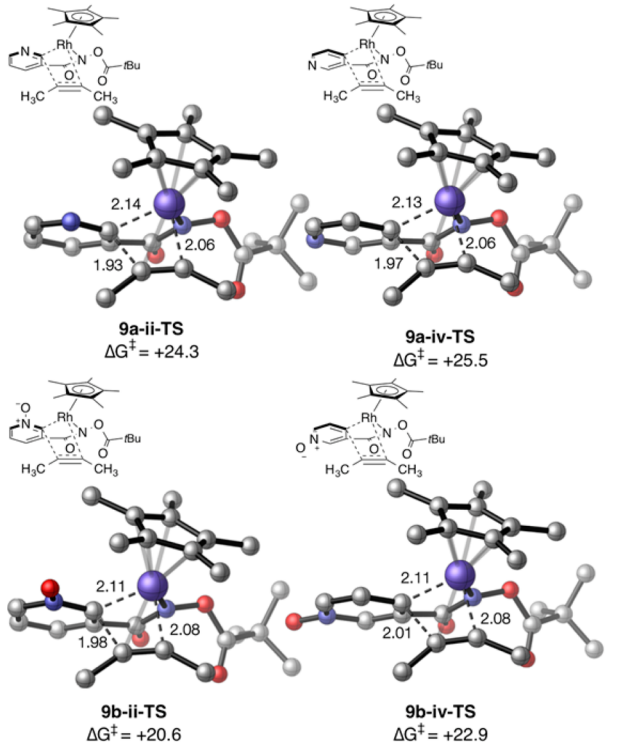

Figure 7. Geometries of the minimum energy alkyne insertion transition structures **9**. Free energies relative to the turnover-determining intermediate (separated reactants for **9a**; complex **4b-iv** for **9b**) are given in kcal mol^{-1} and distances in angstroms.

arene is in close proximity to the electron-deficient (blue) Cp* region of the catalyst fragment and vice versa (electrostatic matching, Figure 6C). Conversely, in the structures for C(4)−H activation, the electrostatics of the Rh−amidate and heteroarene fragments are mismatched (electron-rich near electron-rich and vice versa, Figure 6C). This mismatching is particularly significant with the more polar pyridine *N*-oxide (**5b-iv-TS**). These electrostatic interactions are consistent with the smaller overall dipole moments of the C(2)−H transition structures compared to the C(4)−H TS, due to a "canceling" effect in the former.

Experimentally observed solvent trends are consistent with the proposed role of electrostatic interactions: a weak inverse correlation between site selectivity and solvent polarity is observed in the reaction between **1b** and TES-acetylene (with this alkyne, C−H activation should be selectivity-determining). The C(2):C(4) selectivity ratios in MeCN (ε = 35.7), MeOH (ε = 32.6), 2-PrOH (ε = 19.3), and PhMe (ε = 2.4) are 19:1, 23:1, 31:1, and 47:1, respectively.[10] This solvent effect (albeit weak) is consistent with greater selectivity when a more polar transition state (**5b-iv-TS**) is more destabilized in a less polar solvent.

Origin of Site Selectivity of Alkyne Insertion into C(2)−Rh vs C(4)−Rh. After coordination of an alkyne to the 16-e$^-$ rhodacycles **7** to give complexes **8**, insertion takes place to form a new C−C bond with concurrent cleavage of the rhodacycle $C_{(aryl)}$−Rh bond and formation of a $C_{(alkyne)}$−Rh bond (Figure 1). The minimum energy geometries of the transition states calculated for 2-butyne insertion into the pyridine or pyridine *N*-oxide rhodacycle complexes are shown in Figure 7.

Insertion of 2-butyne at C(2) is more facile than at C(4) for both the pyridine and the *N*-oxide substrates. This energetic trend does not correlate well with the weakness of the C−Rh bond that is being broken in the TS (see Supporting Information): the C(2)−Rh bond of the rhodacycle involving the *N*-oxide is *stronger* than the corresponding C(4)−Rh bond. However, IRC calculations of the alkyne insertion transition states suggest that $C_{(aryl)}$−Rh bond cleavage occurs late (*after* the transition state, Figure 8), and thus $C_{(aryl)}\cdots C_{(alkyne)}$ and $C_{(alkyne)}\cdots$Rh bond formations are more relevant to the energies of the transition states.

Consistent with this, electrostatic interactions between 2-butyne and either the pyridine or the *N*-oxide moiety in the transition state complexes favor insertion into C(2)−Rh over C(4)−Rh (Figure 9). Because the alkyne is initially coordinated to Rh(III) through its π system, it is partially depleted of electron density. In **9a-ii-TS** and **9b-ii-TS**, there is electrostatic matching between the alkyne and the negative potential region of the pyridine or *N*-oxide ring. Conversely, in **9a-iv-TS** and **9b-iv-TS**, the positive alkyne is held in proximity to the positive end of the heteroarene moiety (electrostatic mismatching). In addition, the transition states for insertion into C(2) allow for electrostatic matching between the Cp* and the heteroarene, as described for the C−H activation transition structures. These

DOI: 10.1021/jacs.5b03535
J. Am. Chem. Soc. 2015, 137, 9843−9854

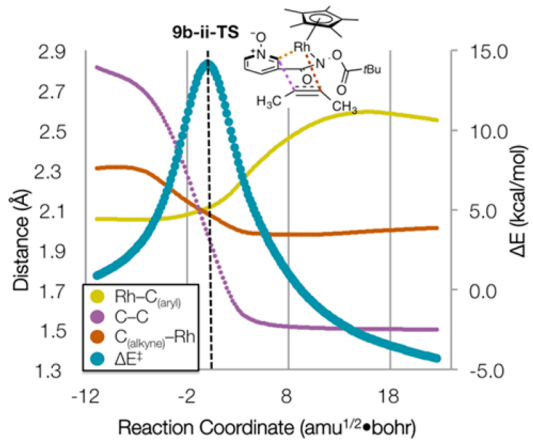

Figure 8. Calculated bond distances and electronic energy along the intrinsic reaction coordinate of 2-butyne insertion into the *N*-oxide–rhodacycle at the 2-position.

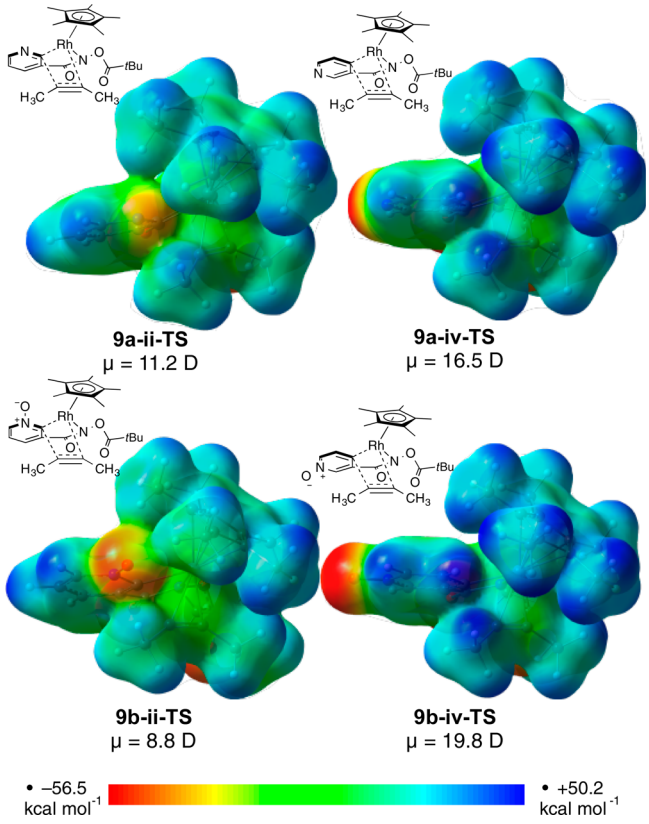

Figure 9. Electrostatic potential surfaces and dipole moments of the transition structures for 2-butyne insertion **9-TS**. Dipole moments calculated in MeOH.

intramolecular interactions, indicated by the electrostatic potential surfaces, are consistent with the much smaller dipole moments calculated for the transition states involving insertion into C(2) compared to C(4).

Role of Electrostatic Interactions in a Substituted Pyridine. The analysis described thus far suggests that electrostatic interactions may play a role in controlling the C(2) vs C(4) site selectivity of both the C–H activation and the alkyne insertion steps of the catalytic cycle. In particular, pyridine *N*-oxide is privileged due to its high degree of polarity compared to pyridine. We hypothesized that if the dipole moment of a pyridine substrate was increased by judicious placement of a substituent, higher C(2)-selectivity could be observed due to electrostatic effects that would resemble that of a pyridine *N*-oxide. To test this hypothesis, we examined 6-trifluoromethylnicotinamide derivative **1e** (Scheme 8). This

Scheme 8. Reaction of 6-Trifluoromethylnicotinamide Substrate 1e with an Alkyne

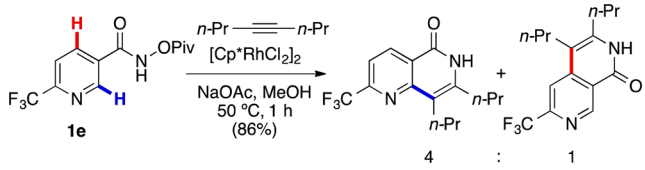

substrate was previously reported to undergo Rh-catalyzed annulation with an alkene resulting in unusually high C(2) site selectivity (see Scheme 2C).[9] The polarity of the trifluoromethyl-substituted pyridine resembles that of the pyridine *N*-oxide due to the strongly electron-withdrawing CF_3 group adjacent to the pyridine nitrogen: the calculated dipole moment of pyridine *N*-oxide in MeOH is 6.8 D, and the dipole moment of 2-trifluoromethylpyridine is 5.7, with a slightly different orientation (Figure 10A). Importantly, because the trifluoromethyl group is *meta* to both C(2) and C(4), it does not affect the sterics at either position, and it should have a similar influence on C–H acidity and C–Rh bond strength at both sites.

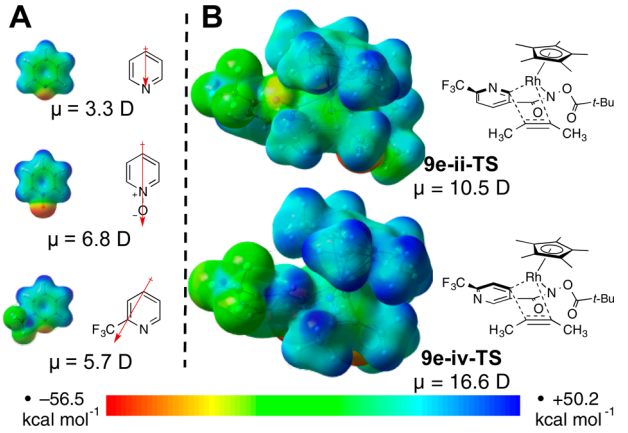

Figure 10. Electrostatic potential surfaces and dipole moments of (A) 2-trifluoromethylpyridine compared to pyridine and pyridine *N*-oxide and (B) the transition structures for 2-butyne insertion into 6-trifluoromethyl-substituted pyridine substrate, **9e-TS**. Dipole moments calculated in MeOH.

In accordance with our prediction, the reaction of **1e** with 4-octyne displays better C(2)-selectivity (4:1, Scheme 8) than the reaction of the unsubstituted pyridine **1a** (1.7:1, see Scheme 3). C(2)–H activation of this substrate is calculated to be slightly favored over C(4) activation by 0.2 kcal mol^{-1}. Although this is only a small preference, it represents a substantial enhancement of C(2)-selectivity for the C–H activation step relative to the unsubstituted pyridine (for which C(4)–H activation is the lower energy pathway by 1.7 kcal mol^{-1}). The reaction selectivity is mostly determined by the alkyne insertion step: insertion of 2-butyne is much more energetically favored at C(2) [$\Delta\Delta G_{(C4-C2)}^{\ddagger}$ = 2.7 kcal mol^{-1}, compared to 1.2 kcal mol^{-1} for the unsubstituted pyridine **1a**]. C(2)-functionaliza-

DOI: 10.1021/jacs.5b03535
J. Am. Chem. Soc. 2015, 137, 9843–9854

tion is calculated to be overall favored by 1.3 kcal mol^{-1} based on the energetic spans for reaction at the two sites (see Supporting Information), corresponding to a predicted product ratio of ~7:1 in very good agreement with the experimentally observed ratio.

Analysis of the electrostatic interactions in the key transition states involving **1e** shows that the Cp* ligand (in both the C−H activation and alkyne insertion steps) and the alkyne (in the alkyne insertion step) have enhanced interactions with the negative-potential end of the trifluoromethylpyridine moiety. Electrostatic potential maps illustrating this phenomenon are shown for the alkyne insertion transition states **9e-TS** in Figure 10B. Consistent with this, the dipole moments calculated for the transition states involving C(2) are much smaller than the dipole moments of those involving C(4).

It is worth noting that sterics can also affect selectivity in biased systems. For instance, 5-methylnicotinamide **1f** undergoes selective C(2)-functionalization with 4-octyne eq 5. The

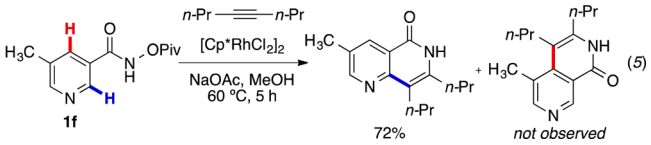

turnover-limiting and selectivity-determining step in this system is calculated to be alkyne insertion, which is strongly favored at C(2) ($\Delta\Delta G^{\ddagger}_{(C4-C2)}$ = 3.1 kcal mol^{-1}; see Supporting Information) despite only a negligible difference in the distribution of electrostatic potential of the methyl-substituted ring compared to the less selective unsubstituted substrate.

Thus, for certain substituted pyridine substrates such as **1e** and **1f**, Rh-catalyzed annulation can be achieved with a synthetically useful degree of site selectivity.[44] However, the use of pyridine *N*-oxides represents a much more general strategy for controlling selectivity that is not substituent-dependent.

CONCLUSIONS

The mechanism and energetics of the Rh(III)-catalyzed (4+2) annulation of *N*-oxide **1b** and its pyridine analog **1a** with alkynes have been studied by DFT calculations. The *N*-oxide substrate is more reactive due to a more favorable amide−Rh interaction in the first half of the catalytic cycle. The turnover-limiting and selectivity-determining step for the reaction of **1b** is either C−H activation or alkyne insertion, depending on the alkyne coupling partner. For pyridine substrate **1a**, C−H activation is the TDTS for functionalization at the 2-position using a dialkyl alkyne, and alkyne insertion is the TDTS for functionalization at the 4-position. Overall, the reaction of pyridine **1a** with a dialkyl alkyne is significantly less selective than the reaction of *N*-oxide **1b** due to nearly identical energy spans for functionalization at both the 2- and the 4-position of the pyridine. On the other hand, both the C−H activation and alkyne insertion steps in the catalytic cycle using *N*-oxide **1b** strongly favor reaction at C(2). The relative importance of various bond-breaking and -forming events to the activation barriers of C−H activation and alkyne insertion were qualitatively assigned from IRC calculations.

Electrostatic interactions favor C(2)−H activation over C(4)−H activation for both substrates (Figure 11). For the *N*-oxide, C−H Brønsted acidity and C−Rh bond strength also favor C(2)−H activation, and these factors work cooperatively

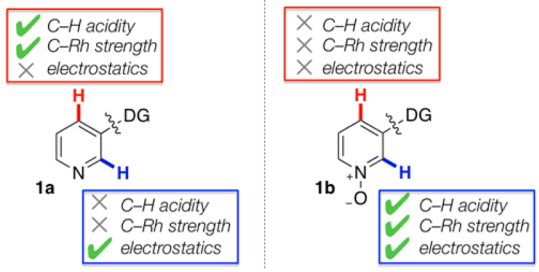

Figure 11. Summary of factors influencing the selectivity of C−H functionalization of **1a** and **1b**. DG = directing group.

resulting in the high site selectivity calculated for the C−H activation step. In contrast, the C(4)−H is the more acidic proton of the pyridine substrate, and a C(4)−Rh bond is stronger than a C(2)−Rh bond. As such, electrostatic interactions vs Brønsted acidity and C−Rh bond strength are opposing influences on the selectivity of pyridine C−H activation. Overall, C−H activation is less selective for pyridine substrate **1a**, and favors the opposite selectivity as does the same mechanistic step for *N*-oxide **1b**.

With internal alkynes, the relative rates of the alkyne insertion step at C(2) vs C(4) are important to the overall site selectivity of the transformation. For both the pyridine and the *N*-oxide substrate, 2-butyne insertion is more facile at C(2). This selectivity can be attributed to favorable electrostatic interactions between the alkyne and the heteroaryl ring, which is particularly significant with the *N*-oxide and with a 6-trifluoromethyl-substituted pyridine derivative.

Importantly, calculation of the complete catalytic cycles using experimentally relevant model systems was critical for accurately predicting selectivities. In studies using acetylene or ethylene as model coupling partners, previous calculations indicated that alkyne or alkene insertion is always fast.[5,16] However, we have found that the use of experimentally relevant substituted alkynes is imperative, as alkyne insertion can be rate-limiting and selectivity-determining. Finally, to our knowledge, the role of electrostatic interactions and polarity on the site selectivity of transition-metal-catalyzed C−H functionalization has not been previously discussed in non-enzymatic systems. Our results suggest that electrostatics can help rationalize phenomena (in particular, site selectivity of metal-catalyzed C−H functionalization) that cannot be completely explained on the basis of other parameters.

ASSOCIATED CONTENT

Supporting Information

The Supporting Information is available free of charge on the ACS Publications website at DOI: 10.1021/jacs.5b03535.

Complete calculated free energy profiles, Cartesian coordinates, electronic energies, entropies, enthalpies, Gibbs free energies, lowest frequencies, experimental procedures, compound characterization, and complete ref 21 (PDF)

AUTHOR INFORMATION

Corresponding Authors

*jhuckins@amgen.com
*othiel@amgen.com
*houk@chem.ucla.edu

DOI: 10.1021/jacs.5b03535
J. Am. Chem. Soc. 2015, 137, 9843−9854

Notes

The authors declare no competing financial interest.

■ ACKNOWLEDGMENTS

This work was supported by the National Science Foundation under the CCI Center for Stereoselective C−H Functionalization (CHE-1205646) and under CHE-1361104 and CHE-1059084. Calculations were performed on the Hoffman2 cluster at UCLA and the Extreme Science and Engineering Discovery Environment (XSEDE), which is supported by the National Science Foundation (OCI-1053575). J.R.H. and O.R.T. gratefully acknowledge Amgen scientist Dr. Tawnya Flick for useful discussions and for assistance with obtaining HRMS data.

■ REFERENCES

(1) For reviews, see: (a) Colby, D. A.; Bergman, R. G.; Ellman, J. A. *Chem. Rev.* **2010**, *110*, 624. (b) Satoh, T.; Miura, M. *Chem. - Eur. J.* **2010**, *16*, 11212. (c) Song, G.; Wang, F.; Li, X. *Chem. Soc. Rev.* **2012**, *41*, 3651. (d) Colby, D. A.; Tsai, A. S.; Bergman, R. G.; Ellman, J. A. *Acc. Chem. Res.* **2012**, *45*, 814. (e) Yamaguchi, J.; Yamaguchi, A. D.; Itami, K. *Angew. Chem., Int. Ed.* **2012**, *51*, 8960.

(2) For seminal examples of analogous reactions using other catalysts, see the following. Ru: (a) Ackermann, L.; Lygin, A. V.; Hofmann, N. *Angew. Chem., Int. Ed.* **2011**, *50*, 6379. (b) Li, B.; Feng, H.; Xu, S.; Wang, B. *Chem. - Eur. J.* **2011**, *17*, 12573. (c) Ackermann, L.; Fenner, S. *Org. Lett.* **2011**, *13*, 6548. Pd: (d) Zhong, H.; Yang, D.; Wang, S.; Huang, J. *Chem. Commun.* **2012**, *48*, 3236. Re/Mg: (e) Tang, Q.; Xia, D.; Jin, X.; Zhang, Q.; Sun, X.-Q.; Wang, C. *J. Am. Chem. Soc.* **2013**, *135*, 4628. Organocatalyst: (f) Manna, S.; Antonchick, A. P. *Angew. Chem., Int. Ed.* **2014**, *53*, 7324.

(3) (a) Ueura, K.; Satoh, T.; Miura, M. *Org. Lett.* **2007**, *9*, 1407. (b) Ueura, K.; Satoh, T.; Miura, M. *J. Org. Chem.* **2007**, *72*, 5362.

(4) (a) Stuart, D. R.; Bertrand-Laperle, M.; Burgess, K. M. N.; Fagnou, K. *J. Am. Chem. Soc.* **2008**, *130*, 16474. (b) Hyster, T. K.; Rovis, T. *J. Am. Chem. Soc.* **2010**, *132*, 10565. (c) Mochida, S.; Umeda, N.; Hirano, K.; Satoh, T.; Miura, M. *Chem. Lett.* **2010**, *39*, 744. (d) Song, G.; Chen, D.; Pan, C.-L.; Crabtree, R. H.; Li, X. *J. Org. Chem.* **2010**, *75*, 7487. (e) Hyster, T. K.; Rovis, T. *Chem. Sci.* **2011**, *2*, 1606. (f) Song, G.; Gong, X.; Li, X. *J. Org. Chem.* **2011**, *76*, 7583.

(5) (a) Guimond, N.; Gouliaras, C.; Fagnou, K. *J. Am. Chem. Soc.* **2010**, *132*, 6908. (b) Guimond, N.; Gorelsky, S. I.; Fagnou, K. *J. Am. Chem. Soc.* **2011**, *133*, 6449. (c) Rakshit, S.; Grohmann, C.; Besset, T.; Glorius, F. *J. Am. Chem. Soc.* **2011**, *133*, 2350. (d) Wang, H.; Glorius, F. *Angew. Chem., Int. Ed.* **2012**, *51*, 7318. (e) Wang, H.; Grohmann, C.; Nimphius, C.; Glorius, F. *J. Am. Chem. Soc.* **2012**, *134*, 19592. (f) Xu, X.; Liu, Y.; Park, C.-M. *Angew. Chem., Int. Ed.* **2012**, *51*, 9372. (g) Hyster, T. K.; Knörr, L.; Ward, T. R.; Rovis, T. *Science* **2012**, *338*, 500. (h) Ye, B.; Cramer, N. *Science* **2012**, *338*, 504. (i) Neely, J. M.; Rovis, T. *J. Am. Chem. Soc.* **2013**, *135*, 66. (j) Hyster, T. K.; Rovis, T. *Synlett* **2013**, *24*, 1842. (k) Ye, B.; Cramer, N. *J. Am. Chem. Soc.* **2013**, *135*, 636. (l) Zhao, D.; Lied, F.; Glorius, F. *Chem. Sci.* **2014**, *5*, 2869. (m) Shi, Z.; Boultadakis-Arapinis, M.; Koester, D. C.; Glorius, F. *Chem. Commun.* **2014**, *50*, 2650. (n) Yu, D.-G.; Azambuja, F.; Gensch, T.; Daniliuc, C. G.; Glorius, F. *Angew. Chem., Int. Ed.* **2014**, *53*, 9650. (o) Hyster, T. K.; Dalton, D. M.; Rovis, T. *Chem. Sci.* **2015**, *6*, 254.

(6) N−N-containing directing group: Zhao, D.; Shi, Z.; Glorius, F. *Angew. Chem., Int. Ed.* **2013**, *52*, 12426.

(7) For a review, see: Patureau, F. W.; Glorius, F. *Angew. Chem., Int. Ed.* **2011**, *50*, 1977.

(8) (a) Zhou, J.; Li, B.; Hu, F.; Shi, B.-F. *Org. Lett.* **2013**, *15*, 3460. (b) Qian, Z.-C.; Zhou, J.; Li, B.; Shi, B.-F. *Synlett* **2014**, *25*, 1036. (c) Cai, S.; Chen, C.; Shao, P.; Xi, C. *Org. Lett.* **2014**, *16*, 3142. (d) Martínez, Á. M.; Rodríguez, N.; Arrayás, R. G.; Carretero, J. C. *Chem. Commun.* **2014**, *50*, 6105.

(9) For two reports in which product was isolated as a single regioisomer, albeit in moderate yield, see ref 8c and the following: Presset, M.; Oehlrich, D.; Rombouts, F.; Molander, G. A. *Org. Lett.* **2013**, *15*, 1528.

(10) Huckins, J. R.; Bercot, E. A.; Thiel, O. R.; Hwang, T.-L.; Bio, M. M. *J. Am. Chem. Soc.* **2013**, *135*, 14492.

(11) Undirected Pd-catalyzed C−H functionalization of pyridine *N*-oxides: (a) Campeau, L.-C.; Rousseaux, S.; Fagnou, K. *J. Am. Chem. Soc.* **2005**, *127*, 18020. (b) Kanyiva, K. S.; Nakao, Y.; Hiyama, T. *Angew. Chem., Int. Ed.* **2007**, *46*, 8872. (c) Cho, S. H.; Hwang, S. J.; Chang, S. *J. Am. Chem. Soc.* **2008**, *130*, 9254. (d) Campeau, L.-C.; Schipper, D. J.; Fagnou, K. *J. Am. Chem. Soc.* **2008**, *130*, 3266. (e) Campeau, L.-C.; Stuart, D. R.; Leclerc, J.-P.; Bertrand-Laperle, M.; Villemure, E.; Sun, H.-Y.; Lasserre, S.; Guimond, N.; Lecavallier, M.; Fagnou, K. *J. Am. Chem. Soc.* **2009**, *131*, 3291. (f) Schipper, D. J.; El-Salfiti, M.; Whipp, C. J.; Fagnou, K. *Tetrahedron* **2009**, *65*, 4977. (g) Wu; Cui, X.; Chen, L.; Jiang, G.; Wu, Y. *J. Am. Chem. Soc.* **2009**, *131*, 13888. (h) Tan, Y.; Barrios-Landeros, F.; Hartwig, J. F. *J. Am. Chem. Soc.* **2012**, *134*, 3683. (i) Xiao, B.; Liu, Z.-J.; Liu, L.; Fu, Y. *J. Am. Chem. Soc.* **2013**, *135*, 616.

(12) Undirected Ni-catalyzed C−H functionalization of pyridine *N*-oxides: Kanyiva, K. S.; Nakao, Y.; Hiyama, T. *Angew. Chem., Int. Ed.* **2007**, *46*, 8872.

(13) Undirected Cu-catalyzed C−H functionalization of a pyridine *N*-oxide: Do, H.-Q.; Daugulis, O. *J. Am. Chem. Soc.* **2007**, *129*, 12404.

(14) Pd-catalyzed C(8)−H functionalization of quinoline *N*-oxides: Hwang, H.; Kim, J.; Jeong, J.; Chang, S. *J. Am. Chem. Soc.* **2014**, *136*, 10770.

(15) For a review on direct functionalization of *N*-oxides, see: Yan, G.; Borah, A. J.; Yang, M. *Adv. Synth. Catal.* **2014**, *356*, 2375.

(16) Computational studies on the reactions of *O*-acyl benzhydroxamic acids with alkenes: (a) Xu, L.; Zhu, Q.; Huang, G.; Cheng, B.; Xia, Y. *J. Org. Chem.* **2012**, *77*, 3017. (b) Wu, S.; Zeng, R.; Fu, C.; Yu, Y.; Zhang, X.; Ma, S. *Chem. Sci.* **2015**, *6*, 2275.

(17) For computational studies on the intramolecular annulation of benzhydroxamic acids with tethered alkynes, see: Quiñones, N.; Seoane, A.; García-Fandiño, R.; Mascareñas, J. L.; Gulías, M. *Chem. Sci.* **2013**, *4*, 2874.

(18) For reviews on computational studies of the mechanism of transition-metal-catalyzed C−H activation, see: (a) Boutadla, Y.; Davies, D. L.; Macgregor, S. A.; Poblador-Bahamonde, A. I. *Dalton Trans.* **2009**, 5820. (b) Balcells, D.; Clot, E.; Eisenstein, O. *Chem. Rev.* **2010**, *110*, 749.

(19) A similar mechanism of C−H activation has been calculated for the Rh-catalyzed annulation reaction of aryl pyrazoles with alkynes: Algarra, A. G.; Cross, W. B.; Davies, D. L.; Khamker, Q.; Macgregor, S. A.; McMullin, C. L.; Singh, K. *J. Org. Chem.* **2014**, *79*, 1954.

(20) Neutral ligand-directed cyclorhodation of arenes and heteroarenes: Carr, K. J. T.; Davies, D. L.; Macgregor, S. A.; Singh, K.; Villa-Marcos, B. *Chem. Sci.* **2014**, *5*, 2340.

(21) Frisch, M. J.; et al. *Gaussian 09*, Revision C.1; Gaussian, Inc.: Wallingford, CT, 2009.

(22) (a) Zhao, Y.; Truhlar, D. G. *Theor. Chem. Acc.* **2008**, *120*, 215. (b) Zhao, Y.; Truhlar, D. G. *Acc. Chem. Res.* **2008**, *41*, 157.

(23) Hay, P. J.; Wadt, W. R. *J. Chem. Phys.* **1985**, *82*, 299.

(24) (a) Gonzalez, C.; Schlegel, H. B. *J. Chem. Phys.* **1989**, *90*, 2154. (b) Gonzalez, C.; Schlegel, H. B. *J. Phys. Chem.* **1990**, *94*, 5523.

(25) (a) Dolg, M.; Wedig, U.; Stoll, H.; Preuss, H. *J. Chem. Phys.* **1987**, *86*, 866. (b) Andrae, D.; Haussermann, U.; Dolg, M.; Stoll, H.; Preuss, H. *Theor. Chim. Acta* **1990**, *77*, 123.

(26) Andrae, D.; Haeussermann, U.; Dolg, M.; Stoll, H.; Preuss, H. *Theor. Chim. Acta* **1990**, *77*, 123.

(27) Marenich, A. V.; Cramer, C. J.; Truhlar, D. G. *J. Phys. Chem. B* **2009**, *113*, 6378.

(28) Scalmani, G.; Frisch, M. J. *J. Chem. Phys.* **2010**, *132*, 114110.

(29) Legault, C. Y. *CYLView, 1.0b*; Université de Sherbrooke, Canada, 2009; http://www.cylview.org.

(30) NMR evidence of cleavage of $[Cp^*RhCl_2]_2$ by acetate: (a) Davies, D. L.; Al-Duaij, O.; Fawcett, J.; Giardiello, M.; Hilton, S. T.; Russell, D. R. *Dalton Trans.* **2003**, 4132. (b) Li, L.; Brennessel, W. W.; Jones, W. D. *Organometallics* **2009**, *28*, 3492.

DOI: 10.1021/jacs.5b03535
J. Am. Chem. Soc. 2015, 137, 9843−9854

(31) Kozuch, S.; Shaik, S. *Acc. Chem. Res.* **2011**, *44*, 101.
(32) Energy span for C(2) = (+20.1) − (−0.5) = +20.6 kcal mol^{-1}. Energy span for C(2) = (+22.4) − (−0.5) = +22.9 kcal mol^{-1}. Note that the TDI is the same for both the 2- and 4-functionalization pathways (**4b-iv**, located at −0.5 kcal mol^{-1} on the free energy surface). This is because **4b-ii** and **4b-iv** are readily interconvertible intermediates (Curtin−Hammett conditions).
(33) Although a lower energy process than alkyne insertion, the oxidation step later in the catalytic cycle is also calculated to have a relatively high reaction barrier (see Supporting Information). Thus, this step is also expected to contribute to catalyst turnover frequency (though not selectivity), and could reasonably become turnover-limiting if the reaction system is changed.
(34) (a) Zhao, Y.; Truhlar, D. G. *Org. Lett.* **2007**, *9*, 1967. (b) Fey, N.; Ridgway, B. M.; Jover, J.; McMullin, C. L.; Harvey, J. N. *Dalton Trans.* **2011**, *40*, 11184. (c) Chen, M.; Craciun, R.; Hoffman, N.; Dixon, D. A. *Inorg. Chem.* **2012**, *51*, 13195.
(35) Interestingly, Rovis et al. have described a related Rh(III)-catalyzed functionalization of a pyridine ring containing a neutral directing group (oxime) at the 3-position that favors C(4)-functionalization:

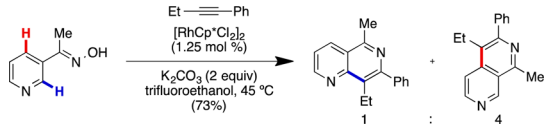

This example may reflect the more facile C(4)−H activation of pyridine in a situation where directed C−H activation is apparently selectivity-determining. (a) Hyster, T. K.; Rovis, T. *Chem. Commun.* **2011**, *47*, 11846. (b) Correction: Hyster, T. K.; Rovis, T. *Chem. Commun.* **2015**, *51*, 5778.
(36) For a review on the properties of pyridine *N*-oxides, including spectroscopic studies comparing them to the properties of pyridine, see: Katritzky, A. R.; Lam, J. N. *Heterocycles* **1992**, *33*, 1011.
(37) In the absence of an alkyne, some deuterium incorporation occurs at both C(2) and C(6) of substrate **1b** (see ref 10). We now believe that the observed exchange at C(6) is facilitated by a different Rh species resulting from catalyst decomposition, as there is no evidence of D incorporation at C(6) in the presence of an alkyne.
(38) Because eq 1 indicates that some isotope scrambling may occur in the reaction with 4-octyne, KIE studies with this alkyne were run in both CH_3OH and CD_3OD. It cannot be ruled out that the smaller KIE seen in both solvents using 4-octyne, compared to using TES-acetyelene, may be partially due to isotope scrambling. However, H/D exchange is only a minor pathway, and the true KIE is expected to be within the range indicated by these experiments.
(39) (a) Gorelsky, S. I.; Lapointe, D.; Fagnou, K. *J. Am. Chem. Soc.* **2008**, *130*, 10848. (b) Gorelsky, S. I.; Lapointe, D.; Fagnou, K. *J. Org. Chem.* **2012**, *77*, 658. (c) Petit, A.; Flygare, J.; Miller, A. T.; Winkel, G.; Ess, D. H. *Org. Lett.* **2012**, *14*, 3680. (d) Gorelsky, S. I. *Coord. Chem. Rev.* **2013**, *257*, 153. (e) Stephens, D. E.; Lakey-Beitia, J.; Atesin, A. C.; Atesin, T. A.; Chavez, G.; Arman, H. D.; Larionov, O. V. *ACS Catal.* **2015**, *5*, 167.
(40) For calculated pK_a values, see Supporting Information.
(41) This trend is consistent with previously calculated pK_a values for pyridine CH acidities: Shen, K.; Fu, Y.; Li, J.-N.; Liu, L.; Guo, Q.-X. *Tetrahedron* **2007**, *63*, 1568.
(42) For studies on the correlation between C−metal and C−H bond strengths, and their relationship to C−H activation, see: (a) Jones, W. D.; Hessell, E. T. *J. Am. Chem. Soc.* **1993**, *115*, 554. (b) Bennett, J. L.; Wolczanski, P. T. *J. Am. Chem. Soc.* **1997**, *119*, 10696. (c) Wick, D. D.; Jones, W. D. *Organometallics* **1999**, *18*, 495. (d) Clot, E.; Mégret, C.; Eisenstein, O.; Perutz, R. N. *J. Am. Chem. Soc.* **2006**, *128*, 8350. (e) Clot, E.; Mégret, C.; Eisenstein, O.; Perutz, R. N. *J. Am. Chem. Soc.* **2009**, *131*, 7817.
(43) Glendening, E. D.; Badenhoop, J. K.; Reed, A. E.; Carpenter, J. E.; Bohmann, J. A.; Morales, C. M.; Landis, C. R.; Weinhold, F. *NBO 6.0*; Theoretical Chemistry Institute, University of Wisconsin, Madison, WI, 2013.
(44) Notably, we have previously found that pyridine substrates with smaller 5-substituents (5-Br, 5-OH, and 5-OMEM) show poor site selectivity during annulation with an *alkene* (norbornene). See ref 10.

DOI: 10.1021/jacs.5b03535
J. Am. Chem. Soc. 2015, 137, 9843−9854